Available online at www.sciencedirect.com
ScienceDirect
Ceramics International 36 (2010) 1797–1803
CERAMICS INTERNATIONAL
www.elsevier.com/locate/ceramint

Consolidation of binderless nanostructured titanium carbide by high-frequency induction heated sintering

In-Jin Shon [a,b,*], Byung-Ryang Kim [a], Jung-Mann Doh [c], Jin-Kook Yoon [c]

[a] Division of Advanced Materials Engineering and the Research Center of Industrial Technology, Engineering College, Chonbuk National University, Chonbuk 561-756, Republic of Korea
[b] Department of Hydrogen and Fuel Cells Engineering, Specialized Graduate School, Chonbuk National University, Chonbuk 561-756, Republic of Korea
[c] Advanced Functional Materials Research Center, Korea Institute of Science and Technology, PO Box 131, Cheongryang, Seoul 130-650, Republic of Korea

Received 25 January 2010; received in revised form 4 February 2010; accepted 4 March 2010
Available online 8 May 2010

Abstract

The rapid sintering of nanostructured TiC hard materials in a short time was investigated with High-Frequency Induction Heating Sintering process. The advantage of this process is that it allows very quick densification to near theoretical density and prohibition of grain growth in nanostructured materials. A dense nanostructured TiC hard material with a relative density of up to 99% was produced with simultaneous application of 80 MPa pressure and induced current of output of total power capacity (15 kW) within 4 min. The effect of the ball milling times on the sintering behavior, grain size and mechanical properties of binderless TiC was investigated.

Keywords: A. Sintering; B. Nanocomposites; C. Hardness; C. Mechanical properties; D. Carbides

1. Introduction

The attractive properties of titanium carbide are high hardness, low density, relatively high thermal and electrical conductivities. TiC is also very stable, with a melting temperature of 2727 K, and does not undergo phase transformations. These properties have seen it used extensively in cutting tool and abrasive materials in composite with a binder metal, such as Ni. But, this binder phase has inferior chemical characteristics to the carbide phase. Most notably, corrosion and oxidation occur preferentially in the binder phase [1]. Hence, the development of binderless TiC is needed to apply in mechanical seals and sliding parts due to its enhanced corrosion resistance.

Nanocrystalline materials have received much attention as advanced engineering materials with improved physical and mechanical properties [2,3]. As nanomaterials possess high strength, high hardness, excellent ductility and toughness, undoubtedly, more attention has been paid for the application of nanomaterials [4,5]. In recent days, nanocrystalline powders have been developed by the thermochemical and thermo-mechanical process named as the spray conversion process (SCP), co-precipitation and high-energy milling [6–8]. However, the grain size in sintered materials becomes much larger than that in pre-sintered powders due to a fast grain growth during conventional sintering process. Therefore, even though the initial particle size is less than 100 nm, the grain size increases rapidly up to 500 nm or larger during the conventional sintering [9]. So, controlling grain growth during sintering is one of the keys to the commercial success of nanostructured materials. In this regard, the high-frequency induction heated sintering (HFIHS) method, which can make dense materials within 2 min, has been shown to be effective in achieving this goal [10–13].

In this work, we investigated the sintering of TiC without the use of a binder by the HFIHS method. The goal of this research is to produce dense fine grained binderless TiC hard material. In addition, we also studied the effect of the initial particle size on the sintering behavior and mechanical properties of binderless TiC.

* Corresponding author at: Division of Advanced Materials Engineering and the Research Center of Industrial Technology, Engineering College, Chonbuk National University, Chonbuk 561-756, Republic of Korea. Tel.: +82 63 2381; fax: +82 63 270 2386.
E-mail address: ijshon@chonbuk.ac.kr (I.-J. Shon).

0272-8842/$36.00
doi:10.1016/j.ceramint.2010.03.007

2. Experimental procedure

The titanium carbide powder with a grain size of <2 μm and 99.5% purity used in this research was supplied by Alfa. The powder was first milled in a high-energy ball mill (Pulverisette-5 planetary mill) at 250 rpm for various periods of time (0, 1, 4, 10 h). Tungsten carbide balls (8.5 mm in diameter) were used in a sealed cylindrical stainless steel vial under an argon atmosphere. The weight ratio of balls-to-powder was 30:1. Milling resulted in a significant reduction of the grain size. The grain sizes of the TiC was calculated from the full width at half-maximum (FWHM) of the diffraction peak by Suryanarayana and Grant Norton's formula [14].

$$B_r(B_{crystalline} + B_{strain})\cos\theta = \frac{k\lambda}{L} + \eta \sin\theta \quad (1)$$

where B_r is the full width at half-maximum (FWHM) of the diffraction peak after instrument correction; $B_{crystalline}$ and B_{strain} are FWHM caused by small grain size and internal stress, respectively; k is constant (with a value of 0.9); λ is wavelength of the X-ray radiation; L and η are grain size and internal strain, respectively; and θ is the Bragg angle. The parameters B and B_r follow Cauchy's form with the relationship: $B = B_r + B_s$, where B and B_s are FWHM of the broadened Bragg peaks and the standard sample's Bragg peaks, respectively. The average grain sizes of the TiC milled for 1, 4 and 10 h determined by Suryanarayana and Grant Norton's formula were about 45 ± 5, 29 ± 4 and 25 ± 4 nm, respectively.

The powders were placed in a graphite die (outside diameter, 45 mm; inside diameter, 20 mm; height, 40 mm) and then introduced into the High-Frequency Induction Heating Sintering (HFIHS) apparatus shown schematically in Fig. 1. The HFIHS apparatus includes a 15 kW power supply, which provides an induced current through the sample, and 50 kN uniaxial press. The system was first evacuated and a uniaxial pressure of 80 MPa was applied. An induced current was then activated and maintained until the densification rate was negligible, as indicated by real-time output of the shrinkage of the sample. The shrinkage was measured by a linear gauge measuring the vertical displacement. The HFIHS can be controlled in two ways: by temperature control or by output control. The latter was chosen to investigate the effect of the output of total power, given that the induced current level has a direct effect on the rate of heating and on the maximum temperature. The output level was 80% output of total power. Temperatures were measured by a pyrometer focused on the surface of the graphite die. At the end of the process, the induced current was turned off and the sample cooled to room temperature. The process was carried out under a vacuum of 5.33 Pa.

The relative density of the sintered sample was measured by the Archimedes method. Microstructural was obtained from samples, which had been polished and etched using Murakami's reagent (10 g potassium ferricyanide, 10 g NaOH, and 100 mL water) for 1–2 min at room temperature. Compositional and microstructural analyses of the products were made through X-ray diffraction (XRD), scanning electron microscopy (SEM) with energy dispersive spectroscopy (EDS) and field emission scanning electron microscope (FE-SEM). Vickers hardness was measured by performing indentations at a load of 49 N and a dwell time of 15 s.

3. Results and discussion

Fig. 2 shows X-ray diffraction patterns of the TiC powder after various milling times. The full width at half-maximum (FWHM) of the diffraction peak is wider with milling time due to strain and refinement of powder. SEM images of TiC powder with milling time are shown in Fig. 3. TiC powder without milling has an angular shape but the processed TiC powder has

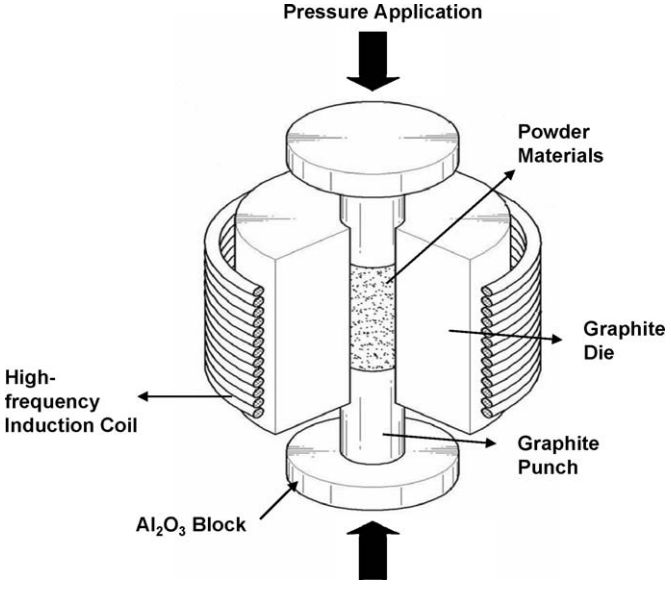

Fig. 1. Schematic diagram of the High-Frequency Induction Heating Sintering apparatus.

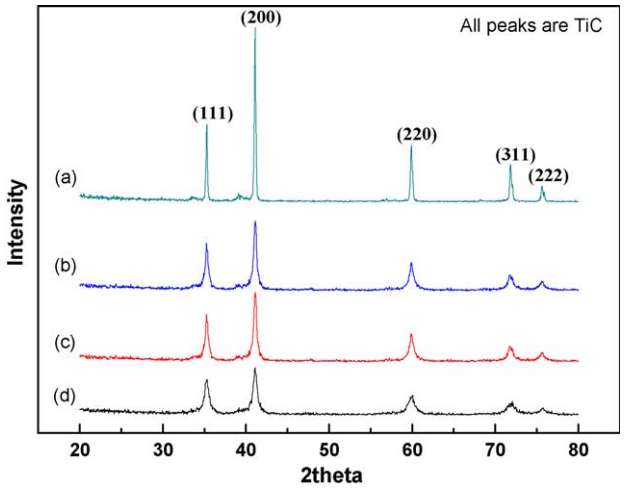

Fig. 2. X-ray diffraction patterns of the TiC powder after various milling times: (a) 0 h, (b) 1 h, (c) 4 h, and (d) 10 h.

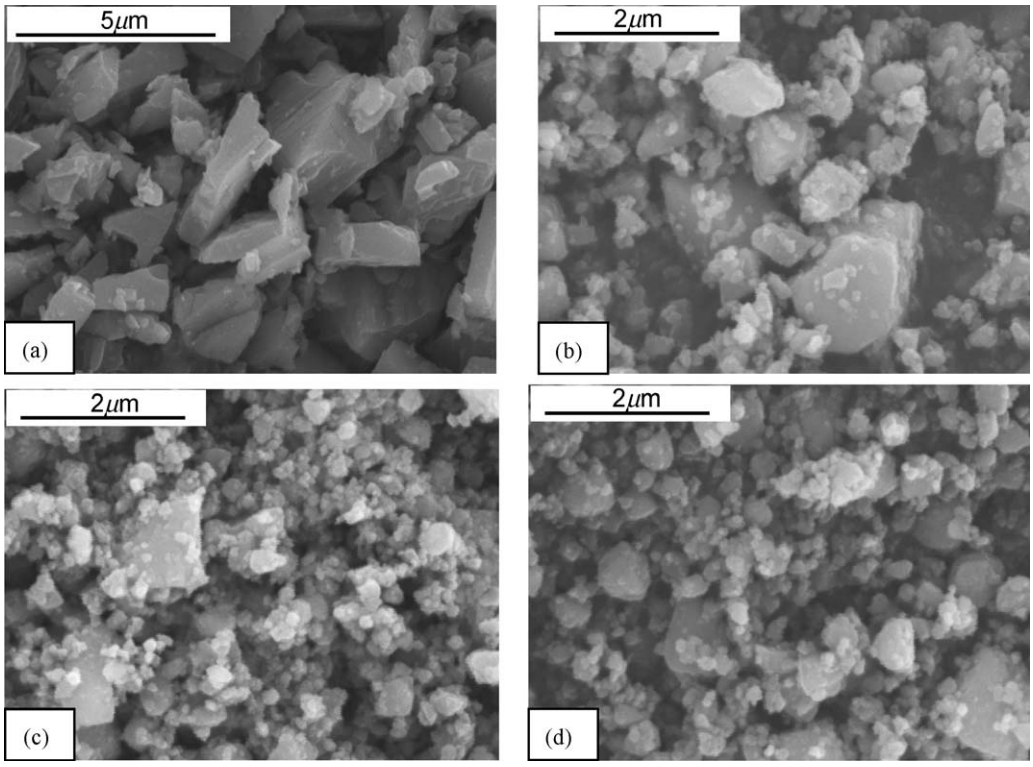

Fig. 3. SEM images of the TiC powders with milling times: (a) 0 h, (b) 1 h, (c) 4 h, and (d) 10 h.

a round shape and refinement with milling time. The variations of the shrinkage displacement and temperature with the heating time for 80% of the total output power capacity (15 kW) during the sintering of the high-energy ball milled TiC under a pressure of 80 MPa are shown in Fig. 4. In all cases, the application of the induced current resulted in shrinkage due to consolidation. The shrinkage initiation temperature varied from 727 to 877 K depending on the milling time. The temperature at which shrinkage started decreased with increasing milling time, and the high-energy ball milling affected the rate of densification and the final density, as will be discussed below. High-energy ball milling treatment allows the control of the formation of compound by fixing the reactant powder microstructure. Indeed, high-energy ball milling produces finer crystallites, strain and defects. Therefore, consolidation temperature

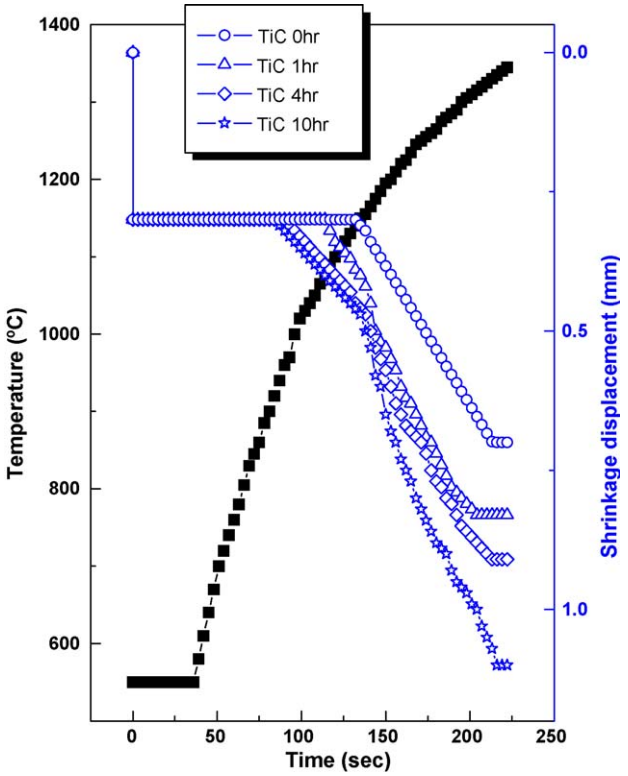

Fig. 4. Variations of temperature and shrinkage with heating time during the sintering of binderless TiC with milling times of 0, 1, 4, and 10 h.

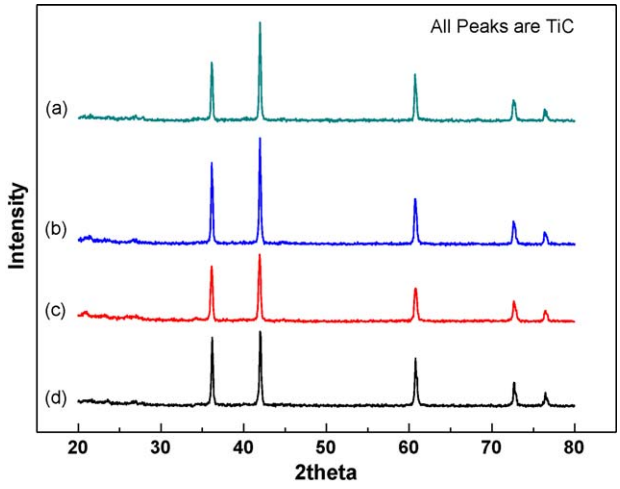

Fig. 5. XRD patterns of binderless TiC sintered from various milled powders: (a) 0 h, (b) 1 h, (c) 4 h, and (d) 10 h.

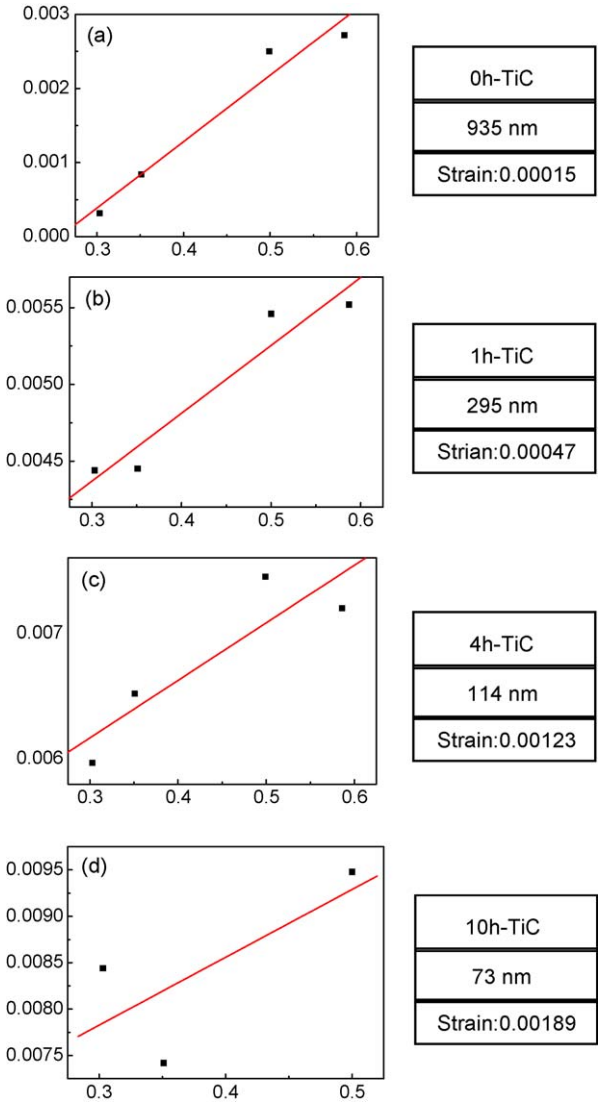

Fig. 6. Plot of $B_r(B_{crystalline} + B_{strain})\cos\theta$ versus $\sin\theta$ for TiC sintered from various milled powders: (a) 0 h, (b) 1 h, (c) 4 h, and (d) 10 h.

decreases with milling time because driving force for sintering and contact points of powders for atomic diffusion increases. Fig. 5 shows the XRD patterns of TiC sintered for all four powders used in this work. All peaks are TiC. Plot of $B_r(B_{crystalline} + B_{strain})\cos\theta$ versus $\sin\theta$ in Suryanarayana and Grant Norton's formula [14] is shown in Fig. 6. The average grain sizes of the TiC calculated from the XRD data were about 935 ± 30, 295 ± 20, 114 ± 15 and 73 ± 10 nm for the samples with milling times of 0, 1, 4, and 10 h and their corresponding densities were approximately 88 ± 3, 97 ± 1, 98 ± 0.5 and $99 \pm 0.5\%$, respectively. Thus, the average grain size of the sintered TiC is not greatly larger than that of the initial powder, indicating the absence of great grain growth during sintering. This retention of the grain size is attributed to the high heating rate and the relatively short term exposure of the powders to the high temperature. As the initial particle size of the TiC powder increased, the porosity also increased. The SEM images of sintered TiC from various milled powders are shown in Fig. 7. The fine pores of TiC sample were decreased with increasing milling time. Fig. 8 shows FE-SEM image of TiC sintered from various milled powders. From the figure, it is known that the grain size of TiC decreases with milling time. The EPMA analysis of TiC sintered from milled powder for 10 h is shown in Fig. 9. Heavier contaminations, such as WC from milling balls and iron from a milling container were not detected in XRD. But a little amounts of iron and Pt were detected in TiC sample from EPMA. The white dots in Fig. 9(b) are Pt because Pt was coated to observe the BSE image. WC was not detected TiC sample. Therefore, a little amounts of heavier contaminations existed in TiC sample.

The role of the current (resistive or inductive) in sintering and or synthesis has been focus of several attempts aimed at providing an explanation to the observed enhancement of sintering and the improved characteristics of the products. The role played by the current has been variously interpreted, the effect being explained in terms of fast heating rate due to Joule heating, the presence of plasma in pores separating powder particles [15], and the intrinsic contribution of the current to mass transport [16–18].

Vickers hardness measurements were performed on polished sections of the TiC samples using a 49 N load and 15 s dwell time. Indentations with large enough loads produced radial cracks emanating from the corners of the indent. The length of these cracks permits the fracture toughness of the material to be estimated using Anstis' expression [19],

$$K_{IC} = 0.016\left(\frac{E}{H}\right)^{1/2}\frac{P}{C^{3/2}} \quad (2)$$

where E is Young's modulus, H is the indentation hardness, P is the indentation load, and C is the trace length of the crack measured from the center of the indentation.

The Vickers hardness of the TiC sintered from ball milled powder for 1, 4 and 10 h were 11.8 ± 0.4, 15.1 ± 0.4, and 25.7 ± 0.5 GPa, and their fracture toughnesses were 8.6 ± 0.5, 7.2 ± 0.4, and 6.1 ± 0.4 MPa $m^{1/2}$, respectively. These values represent the average of 10 measurements. The hardness of TiC with ball milling for 10 h is very high without great reduction of fracture toughness due to refinement of grain.

TiC powder could be synthesized by self-propagating high temperature synthesis (SHS) [20], mechanical alloying (MA) [21,2] and electrothermal combustion [22]. The use of plasma activated sintering to successfully consolidate mechanically alloyed TiC powder has been demonstrated by El-Eskandarany [2]. The mechanically synthesized nanopowder of TiC with an average grain size of 25 nm was consolidated at 1963 K for 4 min under a pressure of 38.2 MPa to a fully dense nanocrystalline TiC with an average grain size of 60 nm. Comparing the above study with ours, the sintering temperature and time of the high-frequency induction heated sintering is lower and shorter than those of plasma activated sintering. The hardness (32 GPa) of TiC studied by El-Eskandarany is higher than that of ours due to refinement of grain size.

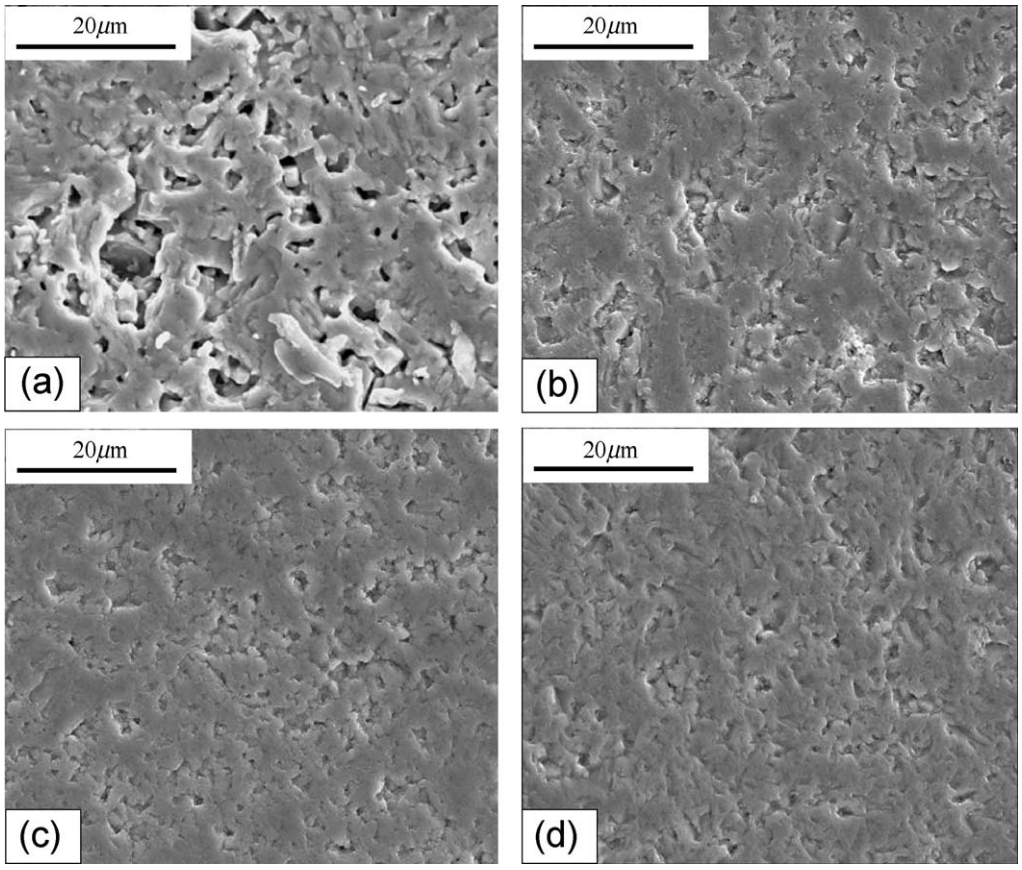

Fig. 7. SEM image of TiC sintered from various milled powders: (a) 0 h, (b) 1 h, (c) 4 h, and (d) 10 h.

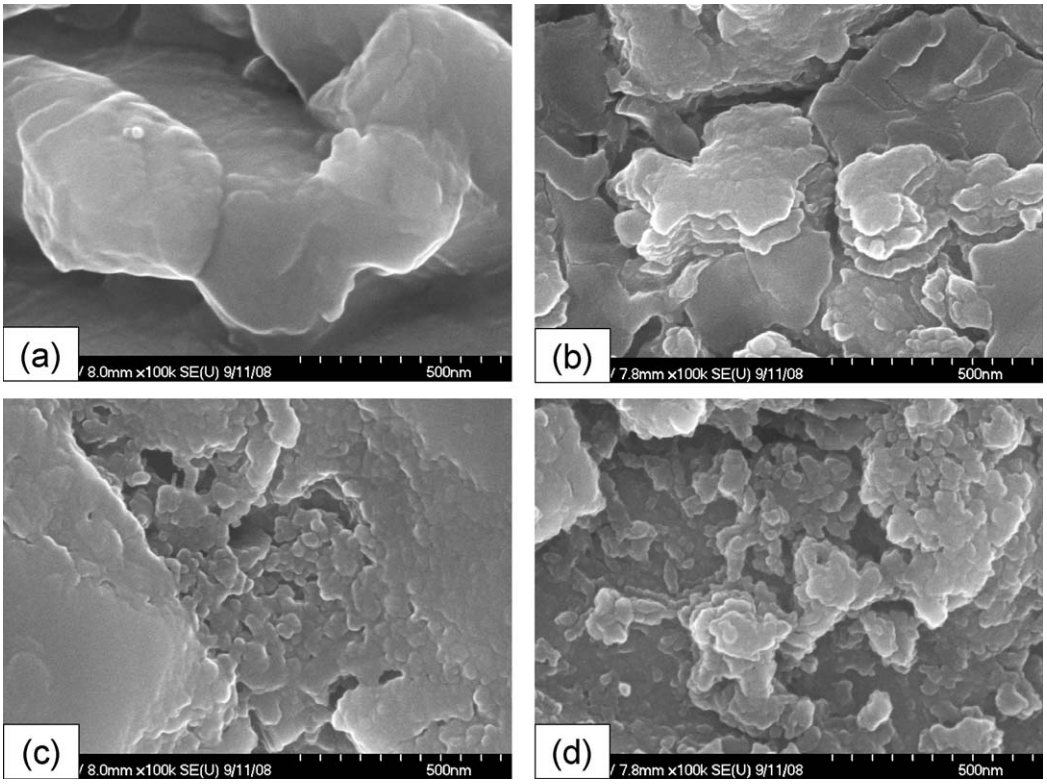

Fig. 8. FE-SEM micrographs of pure TiC sintered from various milled powders: (a) 0 h, (b) 1 h, (c) 4 h, and (d) 10 h.

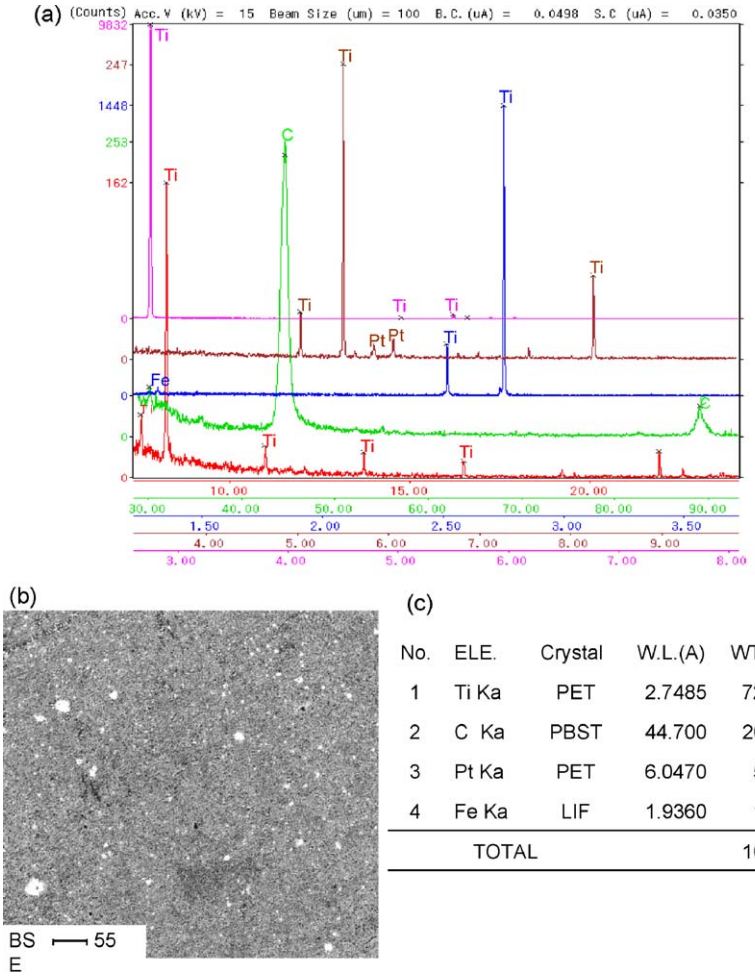

No.	ELE.	Crystal	W.L.(A)	WT(%)	Mol(%)
1	Ti Ka	PET	2.7485	72.16	47.060
2	C Ka	PBST	44.700	20.53	51.262
3	Pt Ka	PET	6.0470	5.94	0.931
4	Fe Ka	LIF	1.9360	1.36	0.747
	TOTAL			100.0	

Fig. 9. EPMA analysis of the pure TiC sintered from milled powder for 10 h: (a) wavelength dispersive X-ray spectroscopy, (b) Back-Scattered Electron image of the binderless TiC and (c) chemical composition of the binderless TiC sample.

4. Summary

Using the rapid sintering method, HFIHS, the densification of binderless TiC was accomplished using high-energy ball milling. Consolidation temperature decreased with milling time because driving force for sintering and contact points of powders for atomic diffusion increased. The average grain sizes of the TiC were about 935 ± 30, 295 ± 20, 114 ± 15 and 73 ± 10 nm for the samples with milling times of 0, 1, 4, and 10 h and their corresponding densities were approximately 88 ± 3, 97 ± 1, 98 ± 0.5 and $99 \pm 0.5\%$, respectively. The Vickers hardnesses of the TiC with ball milling for 1, 4 and 10 h were 11.8 ± 0.4, 15.1 ± 0.4 and 25.7 ± 0.5 GPa, and their fracture toughnesses were 8.6 ± 0.5, 7.2 ± 0.4 and 6.1 ± 0.4 MPa $m^{1/2}$, respectively.

Acknowledgement

This work was supported by a Korea Science and Engineering Foundation (KOSEF) grant funded by the Korea government (MOST) (No. R01-2007-000-20002-0).

References

[1] H. Suzuki, et al., Cemented Carbide and Sintered Hard Materials, Maruzen, Tokyo, 1986, p. 62.
[2] M.S. El-Eskandarany, Structure and properties of nanocrystalline TiC full-density bulk alloy consolidated from mechanically reacted powders, J. Alloys Compd. 305 (2000) 225–238.
[3] L. Fu, L.H. Cao, Y.S. Fan, Two-step synthesis of nanostructured tungsten carbide–cobalt powders, Scr. Mater. 44 (2001) 1061–1068.
[4] K. Niihara, A. Nikahira, Advanced Structural Inorganic Composite, Elsevier Scientific Publishing Co., Trieste, Italy, 1990.
[5] S. Berger, R. Porat, R. Rosen, Nanocrystalline materials: a study of WC-based hard metals, Prog. Mater. 42 (1997) 311–320.
[6] Z. Fang, J.W. Eason, Study of nanostructured WC–Co composites, Int. J. Refract. Met. Hard Mater. 13 (1995) 297–303.
[7] A.I.Y. Tok, L.H. Luo, F.Y.C. Boey, Carbonate co-precipitation of Gd_2O_3-doped CeO_2 solid solution nano-particle, Mater. Sci. Eng. A (2004) 229–234.
[8] I.J. Shon, D.K. Kim, I.Y. Ko, J.K. Yoon, K.T. Hong, Fabrication of nanocrystalline $TaSi_2$–SiC composite by high frequency induction heated combustion synthesis and its mechanical properties, Mater. Sci. Forum 534–536 (2007) 525–528.
[9] M. Sommer, W.D. Schubert, E. Zobetz, P. Warbichler, On the formation of very large WC crystals during sintering of ultrafine WC–Co alloys, Int. J. Refract. Met. Hard Mater. 20 (2002) 41–50.

[10] H.C. Kim, D.Y. Oh, J. Guojian, I.J. Shon, Synthesis of WC and dense WC–5 vol.% Co hard materials by high-frequency induction heated combustion, Mater. Sci. Eng. A 368 (2004) 10–17.
[11] H.C. Kim, D.Y. Oh, I.J. Shon, Sintering of nanophase WC–15 vol.% Co hard metals by rapid sintering process, Int. J. Refract. Met. Hard Mater. 22 (2004) 197–203.
[12] D.Y. Oh, H.C. Kim, J.K. Yoon, I.J. Shon, Simultaneous synthesis and consolidation process of ultra-fine WSi_2–SiC and its mechanical properties, J. Alloys Compd. 386 (2005) 270–275.
[13] H.C. Kim, D.Y. Oh, I.J. Shon, Synthesis of WC and dense WC–*x* vol.% Co hard materials by high-frequency induction heated combustion method, Int. J. Refract. Met. Hard Mater. 22 (2004) 41–49.
[14] C. Suryanarayana, M. Grant Norton, X-ray Diffraction: A Practical Approach, Plenum Press, New York, 1998.
[15] Z. Shen, M. Johnsson, Z. Zhao, M. Nygren, Spark plasma sintering of alumina, J. Am. Ceram. Soc. 85 (2002) 1921–1927.
[16] J.E. Garay, U. Anselmi-Tamburini, Z.A. Munir, S.C. Glade, P. Asoka-Kumar, Electric current enhanced defect mobility in Ni_3Ti intermetallics, Appl. Phys. Lett. 85 (2004) 573–575.
[17] J.R. Friedman, J.E. Garay, U. Anselmi-Tamburini, Z.A. Munir, Modified interfacial reactions in Ag–Zn multilayers under the influence of high DC currents, Intermetallics 12 (2004) 589–597.
[18] J.E. Garay, U. Anselmi-Tamburini, Z.A. Munir, Enhanced growth of intermetallic phases in the Ni–Ti system by current effects, Acta Mater. 51 (2003) 4487–4495.
[19] G.R. Anstis, P. Chantikul, B.R. Lawn, D.B. Marshall, A critical evaluation of indentation techniques for measuring fracture toughness. I. Direct crack measurements, J. Am. Ceram. Soc. 64 (1981) 533–538.
[20] S.K. Mishra, S. Das, R.P. Goel, P. Ramachandrarao, Self-propagating high temperature synthesis (SHS) of titanium carbide, J. Mater. Sci. Lett. 16 (1997) 965–967.
[21] Q. Yuan, Y. Zheng, H. Yu, Mechanism of synthesizing nanocrystalline TiC in different milling atmospheres, Int. J. Refract. Met. Hard Mater. 27 (2009) 696–700.
[22] I.J. Shon, Z.A. Munir, Synthesis of TiC, TiC–Cu composites, and TiC–Cu functionally graded materials by electrothermal combustion, J. Am. Ceram. Soc. 81 (1998) 3243–3248.